 doi:10.20944/preprints202206.0292.v1

*Article*

# Addressed Combined Fiber-Optic Sensors as Key Element of Multi-Sensor Greenhouse Gas Monitoring Systems

**O.G. Morozov[1], J.A. Tunakova[1], S.M.R.H. Hussein[2], A.R. Shagidullin[3], T.A. Agliullin[1], A.A. Kuznetsov[1], B.I. Valeev[1], K.A. Lipatnikov[1], V.I. Anfinogentov[1] and A.Zh. Sakhabutdinov[1*]**

[1] Kazan National Research Technical University named after A.N. Tupolev-KAI, 420111, Kazan, 10 K. Marx St.; microoil@mail.ru (O.G.M.), juliaprof@mail.ru (J.A.T.), taagliullin@mail.ru (T.A.A.), aakuznetsov@kai.ru (A.A.K.), kje.student@mail.ru (B.I.V.) klipatnikov87@mail.ru (K.A.L.), v.anfinogentov@yandex.ru (V.I.A.), azhsakhabutdinov@kai.ru (A.Zh.S.)

[2] University of Kerbala, Kerbala, 56001, Iraq; safaa.mohammed@uokerbala.edu.iq (S.M.R.H.H.)

[3] Research Institute for Problems of Ecology and Mineral Wealth Use of Tatarstan Academy of Sciences 420087, Republic of Tatarstan, Kazan, 28 Daurskaya str.; Artur.Shagidullin@tatar.ru (A.R.Sh.)

*Correspondence: microoil@mail.ru (O.G.M.)

**Abstract:** The design and usage of the addressed combined fiber-optic sensors (ACFOS) and the multisensory control systems of the greenhouse gas concentration on their basis are investigated. The main development trend of the combined fiber-optic sensors (CFOSs), consisting of the fiber Bragg grating (FBG) and the Fabry-Perot resonator (FPR), which are successively formed at the optical fiber end, is highlighted. The addressed fiber Bragg structures (AFBS) usage instead of the FBG in the CFOS leads not only to significant cheapening of the sensor system due to microwave photonics interrogating methods, but also to increasing its metrological characteristics. The structural scheme of the multisensory gas concentration monitoring system is suggested. The suggested scheme allows detecting four types of the greenhouse gases ($CO_2$, $NO_2$, $CH_4$, $O_x$) depending on the material and thickness of the polymer film, which is the FPR sensitive element. The usage of Karunen-Loeff transform (KLT), which allows separating each component contribution to the reflected spectrum according to its efficiency, is proposed. In the future, it allows determining the gas concentration at the AFBS address frequencies. The estimations have shown that the ACFOS design in the multisensory system allows measuring the environment temperature in the range of −60…+300 °C with an accuracy of 0.1–0.01 °C, and the gas concentration in the range of 10…90% with the accuracy of 0.1–0.5%.

**Keywords:** environmental monitoring; greenhouse gases; multi-sensor system; combined fiber optic sensors; fiber Bragg grating; addressed fiber Bragg structure; Fabry-Perot resonator; Carunen-Loeff transforms

## 1. Introduction

The fiber optic sensors (FOS) in the environmental monitoring are of global importance. The growing interest to the FOS is due to their advantages in comparison with the electronic sensors. The FOS have numerous advantages such as a small size, a low weight, a high speed of response to the gas concentration changing, an indifference to the electric and magnetic noises, a remote sensing ability and a resistance to the harsh environmental conditions [1]. Originally, the FOS were developed as the point sensors. A point sensor is less effective compared to a distributed or quasi-distributed sensor array in the amount of information, since it provides data collection from the single control point. The different technologies have been developed to implement multipoint and distributed sensing for this reason [2]. The fibers with etched cladding in the FBG area [3], the plastic optical fibers [4], the Fresnel interferometers with various sensitive coatings were proposed as the sensing elements. The multipoint sensors can also be implemented using the optical fiber sounding methods. These methods have wide functional capabilities, and

 doi:10.20944/preprints202206.0292.v1



most of them show a linear response. However, a number of them are very unstable (due to the interferometric nature of the measurements), and some of them require the expensive peripheral equipment, while others have low reliability in the fiber breaking case (due to the serial connection) [5].

Using the multimode interference effect (MMI) [6,7] is a promising method of the FOS creating. The FOS on MMI principle are convenient because their architecture is simple, they are easy to manufacture and compact. In addition, the spectral response of this class of sensors works like a narrow bandpass filter. In its simplest form, the FOS on MMI includes a section of the multimode fiber (MMF) placed between two single-mode fibers (SMF). These are commonly referred to as "SMF-MMF-SMF" structures [8,9]. Even this simple design allows measuring various physical and chemical parameters such as temperature, humidity, vibration, salinity, pH, etc [10]. The narrowband spectral response of the FOS on MMI can be easily tuned by a wavelength, adjusting its optical and geometrical parameters. The FOS on MMI can be easily used to design a fiber optic multisensory system by wavelength-division multiplexing. Although these sensor systems show a high measurement sensitivity, the multisensory system of this class requires the additional photonic devices to integrate the sensors with the tunable lasers to interrogate them. The additional complexity is in realization of the high reflectivity fiber ends, which is quite difficult to obtain in the infrared spectrum range.

In choosing the direction of sensor development for an environmental monitoring, the focus is on the fiber optic Fabry-Perot end resonators (FPR) [11]. The FPR is the classic sensitive element of pressure [12] and gas or liquid [13–15] concentration sensors. An open FPR for gas concentration control is made by splicing capillary tubes or photonic crystal fibers with the SMF [16]. The open resonator design allows gas flowing freely into the resonator cuvette, which changes the air refractive index between the mirrors. Despite this, the open FPR does not allow measuring the concentration of numerous gases, including greenhouse gases because the change in its concentration is too small to noticeably change the air refractive index between the FPR mirrors. Thus, the key to design the greenhouse gas sensitive element of the FPR is finding or creating the material, refractive index of which is noticeably sensitive to the gas concentration variation [11].

The transparent materials that are sensitive to carbon dioxide ($CO_2$), for example, can be used as the sensitive film of the FPR resonator, where carbon dioxide interacts with the film material and changes its refractive index [17]. However, in practice, the sensors using a functional material are known only in the fiber optic refractometers, basing on the light attenuation effect [18]. The light attenuation coefficient depends on the refractive index of the sensitive film material, which is defined by interaction of the film material with the gas. Thus, the sensor design as the end FPR is characterized by simplicity, usage of inexpensive absorbing materials, and durability. Their design is a relevant task, due to the simplicity of production and use.

Fiber optic sensors (CFOS) based on combination of FBG and FPR for simultaneous gas, temperature, and pressure measurement have recently undergone considerable development [19]. As estimations show, a promising sensitive structure for environmental monitoring should consist of FPR in the form of a thin film at the end face of the optical fiber with FBG near it. The film refractive index is reversibly changed depending on the gas concentration. The interference pattern of the thin-film FPR is sensitive to all environmental parameters, in particular to the changes in temperature, pressure, and gas concentration. The FBG spectrum depends mainly on the temperature, and it has a weak dependence on other external parameters changing. Thus, CFOS allows measuring temperature and gas concentration simultaneously. The problem is that environmental pressure and humidity are usually left out of the measurement [20]. A united CFOS sensor architecture not only serves as an effective method for single-point measurement of the gas concentration and temperature, but also has the great potential for the sensors multiplexing. However, the cost of the system increases significantly due to the switching to a wide spectral

 doi:10.20944/preprints202206.0292.v1



range, which requires usage of the expensive optoelectronic interrogator to separate the spectral responses from FBG and FPR [21].

In order to eliminate the abovementioned problems while preserving the functional advantages, the current work proposes the usage of the Addressed Fiber Bragg Structures (AFBSs) instead of conventional FBGs. AFBS is a fiber Bragg structure which optical response includes two narrowband optical frequencies, while their difference is constant and lies in the microwave frequency range [22–24]. The difference of two optical frequencies is named "address frequency", and it must be unique for each AFBS in the sensor system. A characteristic feature of the AFBS is the invariance of the address frequency under deformation and temperature influence. It allows using the AFBS address frequency for their multiplexing in the sensor array [22]. AFBS performs the triple function in the fiber-optic sensor systems: a sensor; a two-frequency light generator, and a multiplexer. The central wavelength of AFBS can be detected without scanning its spectral range. It is the AFBS key feature. The AFBS interrogation scheme is much simpler compared to a classical optoelectronic interrogation scheme. It consists of a broadband optical light source (e.g., a super luminescent diode), an optical filter with a predefined frequency response with an inclined profile and a photodetector. The AFBS interrogation principle allows combining several AFBS with the identical central wavelengths and the different address frequencies into a unified measurement system [22,25].

The goal of this work is the task statement of designing the addressed combined fiber-optic sensors (ACFOS) as the key element of the multisensory measurement system. ACFOS can be used as the temperature and gas concentration sensors simultaneously. ACFOS is based on AFBS (instead of FBG) combined with FPR, with improved metrological characteristics and possibility of their multiplexing and interrogation in the fiber optic multisensory systems for greenhouse gas monitoring.

To achieve this goal, the following tasks had been formulated:

— the design of ACFOS, based on AFBS and FPR, with analysis of their manufacturing technology (first section);

— the analysis of the principles of separate analyze of the AFBS and FPR responses by temperature and gas concentration based on the sensitivity matrix (second section);

— the analysis of the ACFOS multiplexing principles based on the AFBS address properties and additional spectral analysis of the AFBS and FPR responses to eliminate their cross-distortions using Karunen-Loeff transform (third section);

— the design of the structural scheme and the interrogation principle for the multisensory system for environmental monitoring of the greenhouse gases (the fourth section).

The task formulation for further research themes is in focus of conclusion.

## 2. ACFOS Model

The structural diagram of ACFOS, is shown in Figure 1. ACFOS can be represented as a layered structure consisting of three different layers for broadband laser light propagation: the fiber core; AFBS, consisting of the two homogeneous FBG with close but not equal central frequencies; and FPR. The thin film of the transparent organic polymer material, with thickness $h$, as the gas-sensitive layer of FPR, is applied to the end face of the optical fiber [26]. The film thickness and the polymeric material are selected based on the type of the gas under test. The thin film refractive index depends on the tested gas concentration. The sensors considered in this paper utilize a standard single-mode optical fiber with the core diameter of 8.2 μm, and the core and cladding refractive index of 1.4682 and 1.45, respectively.

The manufacturing of ACFOS can be performed using two technologies similar to the CFOS fabrication technique. Using an ultraviolet continuous laser, the process starts with the two FBG forming. Then FPR is formed at the fiber end face. In some cases, high temperature is required to FPR forming, which can "erase" FBG or its part. For this reason, FPR is usually located at the distance from 1 to 4 cm from AFBS. To reduce this distance, the FBG streaming technique can be used [27,28]. First, FPR is formed at the fiber end face,

Preprints (www.preprints.org) | NOT PEER-REVIEWED | Posted: 21 June 2022 doi:10.20944/preprints202206.0292.v1



then a femtosecond laser is focused through a glass capillary into the core of the fiber for AFBS forming.

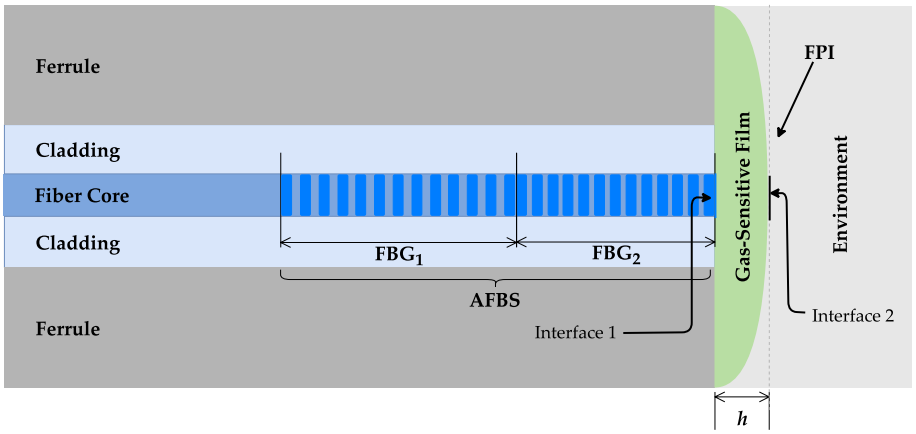


**Figure 1.** The structural diagram of the ACFOS.

To measure the greenhouse gas concentration, the FPR gas-sensitive layer is formed from different polymers: PEI/PVA – for $CO_2$ [29]; polyaniline/$Co_3O_4$ – for CO [30]; $LuBc_2$ – for $NO_2$; PDMS/PMMA – for $NH_3$ [31]; Cryptophane A – for $CH_4$; Cellulose – for $O_X$. Humidity measurement can be performed using PVA coating [32]. It must be noted that the choice of polymers is not limited to the abovementioned types, and the sensors utilizing other polymers can be developed as well. The film thickness is tens of microns. AFBS is formed at the 1550 nm range, due to both the advanced elemental base for the telecommunication systems and the spectral response of polymers and gases in this range.

## 3. The ACFOS Principle

The ACFOS sensor consists of AFBS combined with FPR, which is formed as a polymer film at the fiber end face, Figure 1. FPR consists of two reflective surfaces: the interface between the fiber core and the polymer film (interface 1), and the interface be-tween the polymer film and environment (interface 2). The directed broadband light is initially reflected from AFBS, then the passed light is reflected from FPR. Two reflected beams interfere with each other due to the phase delay caused by the difference in optical paths. Since the reflectivity of the optical fiber end face and the surface of the polymer film are weak, the effect of multiple reflections can be neglected. This allows to consider only the first-order reflected beams. Consequently, the intensity of the ACFOS out-put light can be expressed as a combined spectrum, similarly to [33]:

$$I_{out} \simeq I_{in}\left[\varrho_1 + \varrho_2 + \left(1-\varrho_1-\varrho_2\right)^2 \varrho_{FP}\right], \quad (1)$$

where $\varrho_1$, $\varrho_2$ and $\varrho_{FP}$ are the spectral reflectances of the FBG components of AFBS and FPR, which are defined as [33]:

$$\varrho_i = R_i \exp\left[-\left(\lambda-\lambda_i\right)^2/\omega^2\right], \quad (2)$$

and

$$\varrho_{FP} = 2R_{SMF}\left[1+\cos\left(4\pi L/\lambda+\pi\right)\right],, \quad (3)$$

where $R_i$ are the peak reflectances of the first and second FBG$_i$ ($i = 1,2$, $R_i = 0.6 \div 0.8$), $\lambda_i$ are their central wavelengths and $\omega$ is bandwidth of the FBG, $R_{SMF}$ is the reflectance of the optical fiber end face, $L$ is the FPR length [34]:

$$L = \lambda_1\lambda_2/2\left(\lambda_2-\lambda_1\right), \quad (4)$$

Preprints (www.preprints.org) | NOT PEER-REVIEWED | Posted: 21 June 2022 doi:10.20944/preprints202206.0292.v1



where $\lambda_1$, $\lambda_2$ are the wavelengths of the neighboring maximums of the FPR reflectance spectrum comb.

It is possible to conclude that the resulting ACFOS spectrum is the superposition of the AFBS and the FPR spectra. The sensor response to the gas concentration change can be related with the elastic-optical effect, which leads to the change in the FPR polymer film thickness. The temperature response of the sensor can be explained by the thermal expansion effect and the thermooptic effect of the polymer. The thermooptic effect also changes the FPR wavelength and simultaneously changes the AFBS component wavelengths. The central wavelength shift of the FBG components of AFBS is defined as [22]:

$$\Delta\lambda_i = 2\delta n_{\text{eff}} \Lambda_i , \tag{5}$$

where $\Lambda_i$ are periods of homogeneous sections of the first and second FBG, $\delta n_{\text{eff}}$ is the change in the effective refractive index of the optical fiber core.

Simultaneous measurement of the gas concentration and the temperature, can be made by measuring the comb wavelength of FPR and the central wavelength shift of the FBG components of AFBS. When the wavelengths of the FPR spectral response $\Delta\lambda_{FP}$ and the central wavelengths of the FBG components of AFBS $\Delta\lambda_{AFBS}$ ($\Delta\lambda_{AFBS} = \Delta\lambda_1 = \Delta\lambda_2$, as it follows from the AFBS theory [22]) are determined, the matrix of the sensor sensitivity can be constructed:

$$\begin{bmatrix} \Delta\lambda_{FP} \\ \Delta\lambda_{AFBS} \end{bmatrix} = \begin{bmatrix} K_{FP,C} & K_{FP,T} \\ K_{AFBS,C} & K_{AFBS,T} \end{bmatrix} \begin{bmatrix} \Delta C \\ \Delta T \end{bmatrix}, \tag{6}$$

where $K_{FP,C}$ и $K_{FP,T}$ are FPR sensitivities, and $K_{AFBS,C}$ и $K_{AFBS,T}$ are AFBS sensitivities for the gas concentration and the temperature. The relative values of the gas concentration and the temperature can be obtained from the sensitivity matrix:

$$\begin{bmatrix} \Delta C \\ \Delta T \end{bmatrix} = \frac{1}{M} \begin{bmatrix} K_{AFBS,T} & -K_{FP,T} \\ -K_{AFBS,C} & K_{FP,C} \end{bmatrix} \begin{bmatrix} \Delta\lambda_{FP} \\ \Delta\lambda_{AFBS} \end{bmatrix}, \tag{7}$$

where

$$M = K_{AFBS,T} K_{FP,C} - K_{AFBS,C} K_{FP,T}, \tag{8}$$

is the determinant of the sensitivity matrix.

The matrix coefficients can be determined through measuring the sensor characteristics separately for the temperature and the gas concentration by calibrating the wavelength comb of the FPR spectrum and the AFBS central wavelength.

Simulations of the spectral response of ACFOS with 1 pm resolution between 1520 and 1580 nm have shown that the spectrum (at room temperature and 1 atm pressure) shows ultrahigh spectral contrasts of about 18 and 9 dB for FPR and AFBS, respectively. The reflected spectrum is shown in Figure 2 for the case of a typical concentration of carbon dioxide in the air.

Preprints (www.preprints.org) | NOT PEER-REVIEWED | Posted: 21 June 2022 doi:10.20944/preprints202206.0292.v1



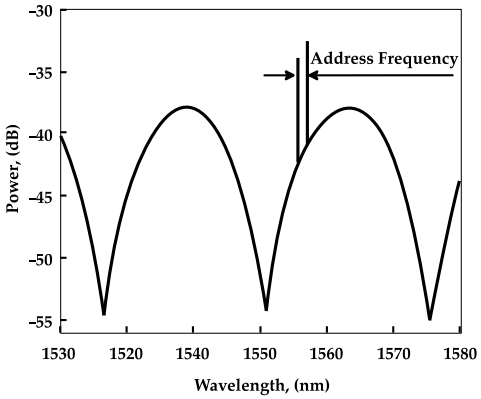


**Figure 2.** CFOS reflected radiation spectrum (laboratory conditions)

## 4. ACFOS Modeling

As it was mentioned above, the AFBS consists of the two homogeneous FBG with close but not equal central frequencies. AFBS can be formed with two FBGs inscribed sequentially or on the same section of the optical fiber [35]. At the same time, it is required that the AFBS has spectral components, the full with at half maximum (FWHM) of which are much smaller than the address frequency of the AFBS [22]. The FWHM of the AFBS spectral components define the width of the address frequency spectrum at the photodetector's output, which in its turn defines the calculation accuracy of the AFBS central wavelength shift. Therefore, the bigger the AFBS physical length, the higher accuracy is provided by it. AFBS formed by two sequential FBGs requires very precise temperature control of the fiber section incorporating the AFBS in order to ensure the constancy of the address frequency. This condition is not always easily met, especially when the AFBS length is several dozens of millimeters. Therefore, the inscription of the two homogeneous FBGs on the same fiber section is a more promising solution.

Despite the presence of the common assumptions and conclusions from the FBG theory, it is preferable to have a complete mathematical model, which could simulate the ACFOS as a whole. A model of a plane electromagnetic wave propagation through a layered structure can be used as a basis for modeling of the optical radiation propagation through the ACFOS [36]. Indeed, an FBG can be represented as a layered structure consisting of numerous homogeneous transparent layers of silica glass with alternate refractive index. The AFBS model is formed by two FBGs with different grating periods located sequentially or in the same fiber section. FPR is modelled as the final homogeneous transparent layer with the parameters of the gas-sensitive film. The Cartesian coordinate system with the origin at the beginning of the AFBS is chosen for modeling [36]. Then for the plane electromagnetic wave propagation, the continuity of the electromagnetic field is required. This implies that the electric and the magnetic fields are equal at each optical layer interface:

$$\begin{cases} E_i(z_i) = E_{i+1}(z_i) \\ H_i(z_i) = H_{i+1}(z_i) \end{cases}, \; i = 0, N-1, \tag{9}$$

where $E_i$ and $H_i$ are the vector magnitudes of the electric and magnetic fields, respectively; $i$ is the layer number, so that $i = 0$ is the layer of silica fiber from the optical source to the AFBS, $i = 1$, $N - 2$ are the layers of alternate refractive index, $i = N - 1$ is the layer of the gas-sensitive film, $i = N$ is the layer of environment. For the plane electromagnetic wave, the system of equations (9) is formulated as follows:

Preprints (www.preprints.org) | NOT PEER-REVIEWED | Posted: 21 June 2022 doi:10.20944/preprints202206.0292.v1



$$\begin{cases} t_i \cdot e^{-j\kappa_i z_i} + r_i \cdot e^{j\kappa_i z_i} = t_{i+1} \cdot e^{-j\kappa_{i+1} z_i} + r_{i+1} \cdot e^{j\kappa_{i+1} z_i} \\ \dfrac{t_i \cdot e^{-j\kappa_i z_i} - r_i \cdot e^{j\kappa_i z_i}}{w_i} = \dfrac{t_{i+1} \cdot e^{-j\kappa_{i+1} z_i} - r_{i+1} \cdot e^{j\kappa_{i+1} z_i}}{w_{i+1}} \end{cases}, \; i = 0, N-1. \tag{10}$$

Here $t_i$ and $r_i$ are the transmittance and reflectance of each layer, $z_i$ are the coordinates of the interfaces between layers, $k_i$ is the wavenumber and $w_i$ is the wave impedance of each layer:

$$\begin{aligned} \kappa_i(\lambda, \varepsilon_i, \mu_i) &= \frac{2\pi}{\lambda}\sqrt{\varepsilon_i \mu_i} = \frac{2\pi}{\lambda} n_i, \\ w_i(\mu_i, \varepsilon_i) &= \sqrt{\mu_i \mu_0 / \varepsilon_i \varepsilon_0} \end{aligned}, \tag{11}$$

taking into consideration that $c\sqrt{\varepsilon_0 \mu_0} \equiv 1$, where, $\lambda = c/f$ is the wavelength, $\omega = 2\pi f$ is the circular frequency, $\varepsilon_i$ is the permittivity and $\mu_i$ is the permeability of the layer, which are determined by the corresponding coefficients of the layers, multiplied by the absolute permittivity $\varepsilon_0$ and the absolute permeability $\mu_0$ of the vacuum, c is the light speed in vacuum.

The system of equations (10) provides $2 \cdot N$ equations for finding the $2 \cdot (N + 1)$ unknown quantities. It is assumed that all wave intensity that comes from the light source into the first layer passes through it without loss and there is no reflection from the far boundary of the third layer. These conditions make it possible to determine the reflection and transmission coefficients for the zero and the last layers ($t_0 = 1$, $r_{N+1} = 0$). Hence, we obtain a system of $2 \cdot N$ linear equations for $2 \cdot N$ unknown complex variables $r_i$, $t_i$.

The solution of the system of equations allows to define the transmittance and reflectance for each layer at any wavelength. The solution of the system of equations for each wavelength in a particular range enables complete modeling of the AFBS reflectance spectrum.

The system of equations (10) is initially formulated on condition that the layer interfaces coincide with the chosen coordinate grid $z_i$. In this case, as it was mentioned before, $z_i$ is chosen so that at $i = 1, N - 2$ they would form layers with alternate refractive indices. Such choice of the coordinate grid is convenient for the homogeneous layer calculation. However, this approach is problematic in the case of modeling of two periodic structures formed on top of each other, since it is not possible to impose two periodic structures with different periods on the same coordinate grid.

On the other hand, the conditions of electromagnetic field continuity are met not only at the interface between layers but also in every point of electromagnetic wave propagation. This fact allows to use the coordinate grid $z_i$ that does not coincide with the layers' interfaces.

The induced refractive index of the optical fiber changes harmonically. Therefore, if the coordinate grid does not coincide with the layers of periodic structure, it is necessary to define the value of the induced refractive index for each layer. For that, it is sufficient to define the permittivity of each layer, superimposing the periodical variation of $\varepsilon_i$ on the arbitrary uniform coordinate grid under the assumption that the permeability of all the layers is equal to one:

$$\varepsilon_i = \left( \left( n_0^2 + n_1^2 \right) + \frac{\pi}{2} \left( n_0^2 - n_1^2 \right) \sin\left( \frac{2\pi}{\Lambda} \cdot \frac{z_{i+1} + z_i}{2} \right) \right) \frac{1 - j \cdot \tan(\alpha)}{2}, \tag{12}$$

where $n_0$ and $n_1$ are the refractive indices of the FBG layers, $\Lambda$ is the FBG period, $\tan(\alpha)$ is the dielectric loss tangent of the optical fiber, $z_i$ is the arbitrary coordinate grid.

The convenience of the arbitrary coordinate grid usage lies in the fact that by adding other summands with different period of harmonic variation of the refractive index to the equation (12), it is possible to model any number of FBGs inscribed on the same section of the optical fiber. The usage of the coordinate grid which is not linked up to the FBG period

Preprints (www.preprints.org) | NOT PEER-REVIEWED | Posted: 21 June 2022 doi:10.20944/preprints202206.0292.v1



makes it possible to model various ACFOS configurations with different address frequencies and to obtain the values of the induced refractive index change along the optical fiber for ACFOS point-by-point inscription with the desired spectral response.

Figure 3 shows the results of the numerical simulation of the ACFOS spectral response using the mathematical model introduced above. The address frequency of the ACFOS is 80 GHz.

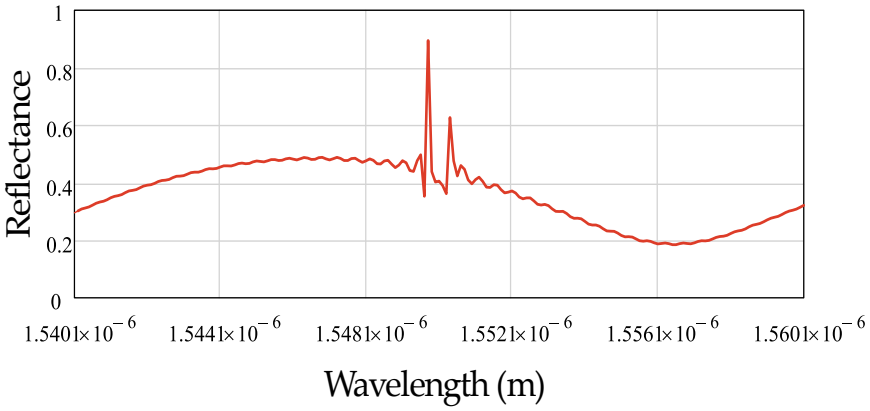


**Figure 3.** ACFOS reflected radiation spectrum (numerical simulation)

As it can be seen from Figure 3, the ACFOS spectrum response is comprised of a sinusoid-like spectral shape formed by the Fabry-Perot cavity and two narrow peaks formed by the FBGs. It must be noted that the spectral response contains dips near the reflection peaks of the FBGs, which can be explained by the interference of waves reflected from the FBG, which received a phase shift when passing through the Fabry-Perot cavity.

Using the proposed mathematical model, it is possible to study the nonuniform heating of the ACFOS along its length, to analyze the usage of chirped and complex apodized FBGs in the structure of ACFOS; the model also enables studying the spectral response variation due to the gas concentration and temperature influence on the sensor.

## 5. ACFOS Multiplexing

The sensor multiplexing is based on the address measuring conversion for the AFBS, namely: "the AFBS central wavelength – the difference frequency between the first and the second FBG components of AFBS – the photodetector output beat frequency – the AFBS microwave frequency address". Simulations of the AFBS sensors with different address frequencies were performed. The dependence of the address frequencies on the grating period of the constituent FBGs in the range up to 20 GHz was obtained (Figure 4). The address frequencies of 8, 15.6, and 19.2 GHz were obtained. The dependence of AFBS spectral response on the FBG length was also established, as shown in Figure 4,*d*). With the increase of FBGs lengths, their reflectance also increases. Therefore, a tradeoff between the sensor length and the reflectance must be achieved. The dependences clearly demonstrate the possibility of the sensor multiplexing in a narrow wavelength range compared to the operating wavelength of 1550 nm with full addressability.

Numerical experiments for the multisensory gas concentration control system were performed in the Optiwave System software. The sensor addressability was determined by the nonequivalent conditions of the AFBS address frequencies $\Omega_k \neq \Omega_j$, where $k$ and $j$ are the indexes of AFBS in the sensor array, $k, j \in N$, and $N$ is the number of AFBS. The difference $|\Omega_k - \Omega_j|$ also must not be equal or multiple to each of the address wavelengths $\Omega_k$ and $\Omega_j$ [24].

The frequency difference between two neighboring sensors is about 100 MHz. If the address frequencies of ACFOS do not exceed 20 GHz and the sensor number is no more than 200, then they can be differenced by the Fast Fourier Transform. The sensor number

 doi:10.20944/preprints202206.0292.v1



will be less, if the bandwidth is decreased to 120 MHz (which is corresponded to the FBG recording technology with a minimum bandwidth of 1 pm [37]). The existing methods of the AFBS central wavelength determining, based on the optical filter with an inclined profile [22] and based on the Fast Fourier Transform [25], allow determining the absolute temperature with an error not exceeding ±0.1 °C and ±0.01 °C respectively. The main condition of the accurate temperature determination is equality of the reflection coefficients $R_i$ of both FBGs forming ACFOS. The ACFOS spectrum is a superposition of the AFBS and FPR spectra, hence, the condition of equality is not fulfilled.

Preprints (www.preprints.org) | NOT PEER-REVIEWED | Posted: 21 June 2022 doi:10.20944/preprints202206.0292.v1



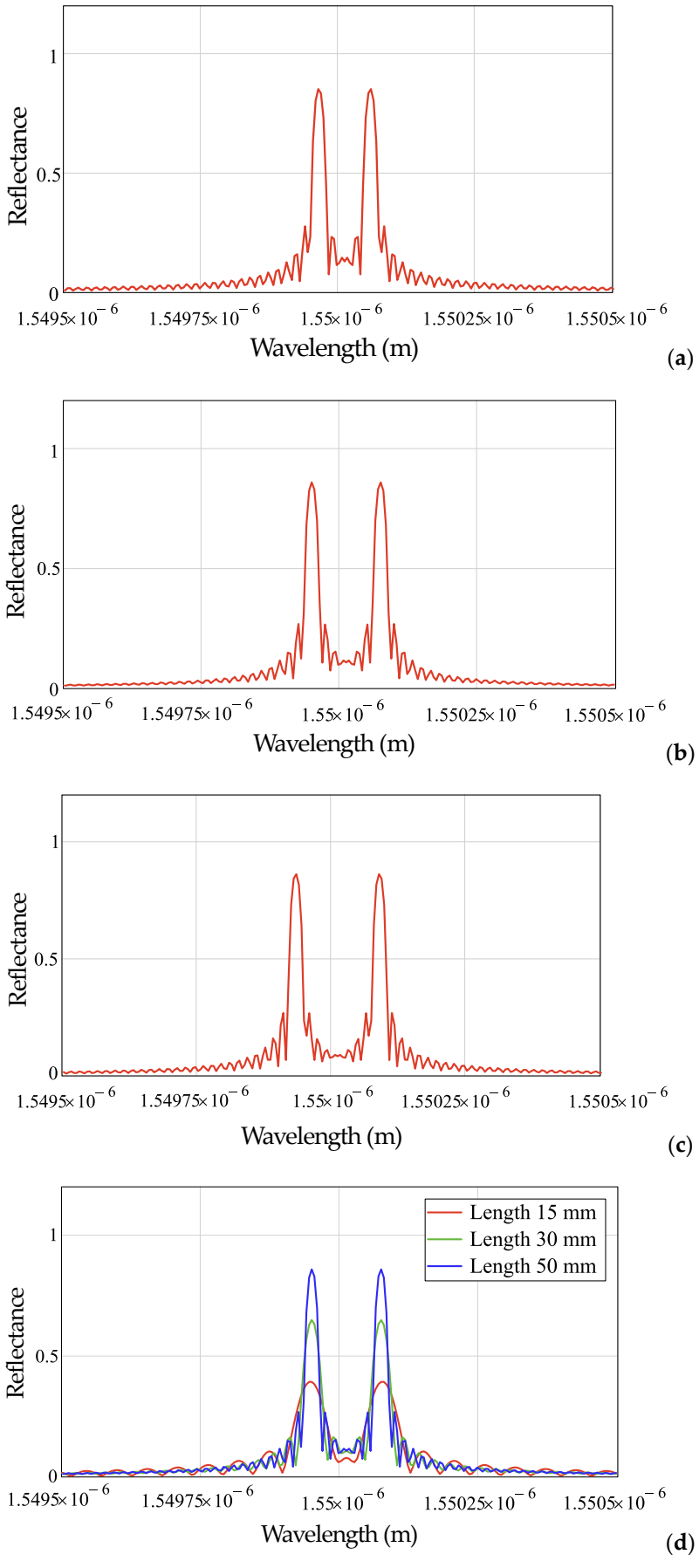


**Figure 4.** Simulation results of AFBS with two FBGs. AFBS address frequencies: (a) 8 GHz, (b) 15.6 GHz; (c) 19.2 GHz; (d) Length variation of both FBGs

 doi:10.20944/preprints202206.0292.v1



Karunen-Loeff transform (KLT) can be used to solve this problem [38]. The ability of KLT to separate the FBG and the FPR spectra can be successfully used for interrogation of the ACFOS spectrum. This is a common procedure used in multisensory systems for oil, gas and geothermal engineering, where the combined sensors operate in the temperature range from – 60 to 300 °C and high pressure (up to 100 atm). The KLT procedure is also applicable for environmental monitoring, where the conditions are similar in temperature and in gas concentration changes from 10 to 90%.

The data separation from seven sensors is demonstrated in [21]. The first five sensors are the FBGs with the similar reflection coefficients. They are uniformly distributed in 1550 nm range, and have different reflection amplitude at the central wavelength due to the overlap with the FPR spectrum. The sixth sensor is the external FPR with a maximum reflectance of 33% and the resonator length of 25 μm, designed to control the external influences. Finally, the seventh sensor is the weakly reflective FPR (0.95%) which simulates a pressure sensor. The total ACFOS reflectance spectrum has the width of 60 nm. After KLT is applied, the components of each sensor are separated, while all FBGs have equal reflection amplitudes.

The KLT algorithm usage can change the structure of wave multiplexing multisensory systems, in particular for the high density sensors [39]. The typical principle of such systems is based on the wavelength separation, assigned as the sensor work range. This approach is very vulnerable due to the spectra overlapping possibility. We eliminate this disadvantage by using AFBS, which can also operate at the common central wavelength [24]. In additional, the KLT algorithm usage allows eliminating the ambiguity of the sensor readings, since each sensor is encoded in its spectrum part.

The discussion in this section represents the first step towards combining the address-based approach in ACFOS with the KLT algorithm. The goal statement for further research is to investigate the possibility of applying of two-, three-, and four-component AFBS [24,25,38] with a strongly reflective FPR for the temperature compensated gas concentration measurements and with a weakly reflective FPR for ambient pressure compensation.

## 6. Multisensory Environmental Monitoring System

Let us focus on the task statement of the ACFOS multisensory system creating, the core of which must be an interrogator. The design of the interrogator is important, not only because it determines the system performance and the measuring conversion principle, but also because it must ensure its working ability not only in the laboratory, but also in the field conditions. For ACFOS, the system requirements are as follows.

*Physical requirements:* The optical fibers guarantee small sensor size, easy-to-lay cable, and lightweight construction. Small size is essential for environmental applications where the key requirement is minimizing the control point size.

*Metrological requirements:* Most ACFOS provide high conversion accuracy, linear calibration function and fast response.

*System requirements:* ACFOS enables multisensory architectures in which sensors can be fabricated on a single fiber or combined across different topologies into a single interrogation system. ACFOS allows constructing the quasi-distributed measurement systems with high spatial resolution.

*The field measuring systems must comply with the following requirements:* the interrogator cost must be limited by its specific application; the size, weight, and shape of the interrogator must match the size of the rack of the automatic air pollution monitoring station; it must have low-power consumption with the battery power backup; the data recording rate for each channel must be 10 times more than the possible variation of the measured value; the number of ACFOS must be determined by the measuring requirements.

The most important factor of any measuring system is its cost. The cost depends on many factors. The subsystem that has a dominant part of the cost is usually determined by its functional purpose. In some applications, a fiber cost may be dominant, in others

Preprints (www.preprints.org) | NOT PEER-REVIEWED | Posted: 21 June 2022 doi:10.20944/preprints202206.0292.v1



the multiplexing scheme. In the sensor systems, the interrogator typically has a dominant part of the cost. In [22,25] we show that the cost of the microwave photonic interrogators for AFBS can be in tens of times less than the classical optical-electronic interrogator cost. Consequently, the main challenge for the system developers is to obtain information about the FPR shift on the address frequencies of the sensor using the KLT algorithm.

The structural diagram of the designed system working on the reflection principle is shown in Figure 5. The sensors (6.1) – (6.N) are mounted remotely, and the microwave photonic interrogator is mounted in the automated control rack. The light source (1) is a broadband laser diode (LD) in the range of 1550 nm. Its temperature must be stabilized by the thermoelectric controller, which is critical to ensure stable output power of the light source over the operating wavelength range. The optical radiation from the source (1) is divided into two channels by means of fiber-optic splitter (2) in order to compensate possible instabilities in the LD output power through the normalization of the signal amplitudes in both channels. In the channel 1, the reflected radiation from the ACFOS sensors (6.1) – (6.N) connected through the splitter (5) is directed to the photodetector (7.1) through the optical circulator (4.1), while the source (1) is isolated from the reflected radiation by optical isolator (3.1) (>20 dB). Each ACFOS can use FPR with different polymer films. The output signal of the photodetector (7.1) is converted by means of the analog-to-digital converter (ADC) (8.1) and processed by the computer (10). Similarly, in the channel 2, the radiation reflected from the reference sensor (9) is guided to the photodetector (7.2) through the circulator (4.2), while the source being isolated from it with the isolator (3.2). The reference sensor (9) has the reference spectrum equal to the spectrum of the measurement sensor at the calibration points. It allows additional consideration of variations in LD parameters. The output signal of the photodetector (7.2) is also converted by the second ADC (8.2) and processed be the computer (10).

The ACFOS packaged design in the ferrule is shown in Figure 6,*a*. The overall design of the microwave photonic interrogator (MPI), considering the functional electronics and the commutation fibers, is shown in Figure 6,*b*. In addition, the Ibsen I-MON optical-electronic interrogator, using to control and compare measurement results, is installed in the housing.

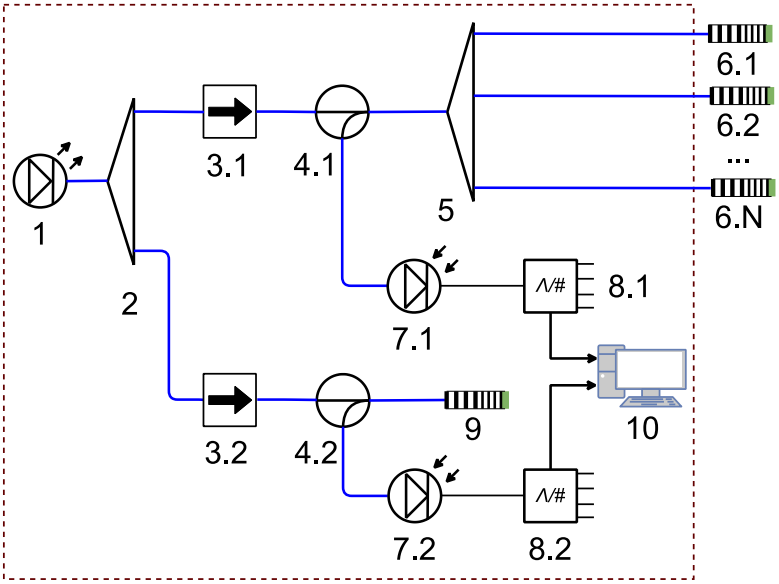


**Figure 5.** Schematic diagram of a multi-sensor greenhouse gas monitoring system: (1) wideband light source, (2) and (5) fiber-optic splitters, (3.1) and (3.2) optical isolators, (4.1) and (4.2) fiber-optic circulators, (6.1) – (6.N) ACFOSs, (7.1) and (7.2) photodetectors, (8.1) and (8.2) ADCs, (9) reference sensor, (10) computer.

Preprints (www.preprints.org) | NOT PEER-REVIEWED | Posted: 21 June 2022 doi:10.20944/preprints202206.0292.v1



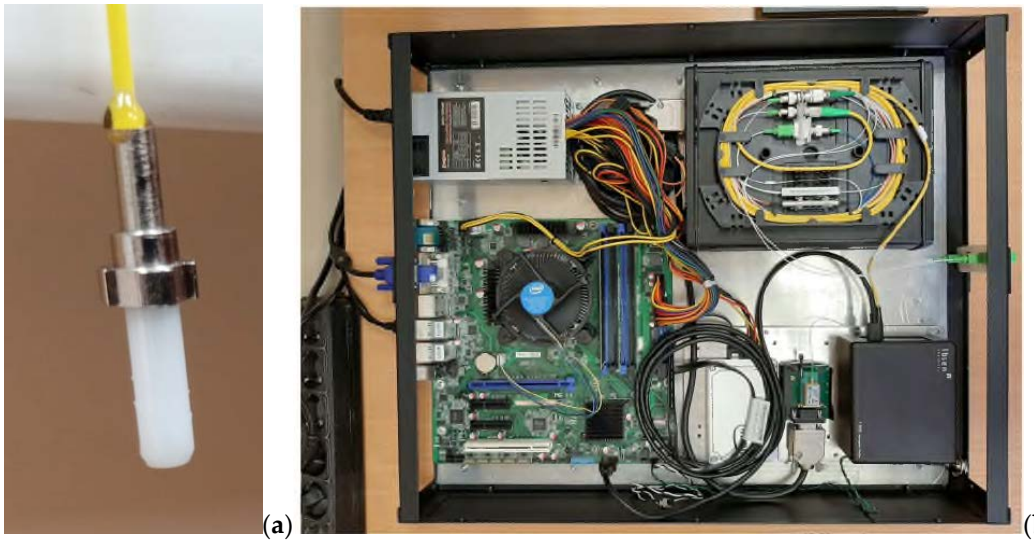

**Figure 6.** A prototype of CFOS (a) and interrogator (b) for a multi-sensor system

MPI consists of the following nodes:

1) Optical-electronic module (OM) of microwave photonics type;

2) Cross-1 (KP1) (for switching the optical-electronic module with sensors through a fiber optic cable);

3) Cross-2 (KR2) (for splitting the fiber optic cable for 24 channels for sensor connecting);

4) Fiber optic cable connecting the KP1 and KP2;

5) Patch cords for connecting the RC2 and ACFOS.

The usage of the non-electrical measuring instruments and the fiber-optic cable allows applying MPI for environmental monitoring at the energy, oil and gas, chemical industries (including manufacturing with aggressive gases), metallurgical enterprises, and in medicine.

ACFOS, that are not included in MPI kit, consist of electrically non-conductive materials, which allows using them in the high voltage areas. In addition, they are manufactured in the enclosure, which is not susceptible to corrosion. ACFOS are also immune to electromagnetic noises and do not interact with other electrical devices. They can be used safely in potentially explosive environments without risk of sparks. The sensors have the high accuracy and the wide operating temperature range from −60 to +300 °C, depending on the type of fiberglass cable protection. If necessary, it is possible to combine (multiplex) numerous sensors into one measurement network, with the measurement module, placed at the distance up to 10−30 km. Estimations have shown that the ACFOS design and system as a whole allows measuring the gas concentration in the range of 10−90% with an error of 0.1−0.5%.

The ACFOS undoubted advantages are their high speed, passivity, resistance to electromagnetic noises, dielectric nature, fire safety, low weight and dimensions, operability in a wide temperature range and interference immunity of the data transmission channel. This approves the possibility of building on their basis promising tools and multi-sensor systems for environmental monitoring of green-house gas concentrations.

## 7. Conclusions

As the result of this research, the concept of development of multisensory systems for environmental monitoring of greenhouse gases of various levels is developed. The concept allows by 2030 forming a deployed network of control posts for enterprises, regional formations and the whole country. The proposed concept is based on the current level of information technology and computational tools, which allows improving sys-

tems of monitoring and management of the environmental situation. Intelligent technologies and monitoring means based on fiber optic technologies should become the priority directions for increasing the ecological safety level. To create an intelligent system of the greenhouse gas monitoring is necessary to solve the tasks of creating workable in the field conditions:

– the address CFOS, based on AFBS and FPR, capable to distinguish the gas type, determine its concentration, have a built-in system of temperature, atmospheric pressure and ambient humidity compensation;

– the microwave photonic interrogator for construction of multisensory system of ecological greenhouse gas monitoring, possessing possibility of control of ACFOS address and analysis reflection from them in the narrowband, limited by AFBS address frequencies, with transformation into digital data package;

– the multisensory system software to process a digital data package allowing separate registering of AFBS and FPR responses for gas concentration, temperature, pressure and ambient humidity based on the single multi-parameter sensitivity matrix and Karunen-Loeff transformation algorithms to eliminate cross-distortions;

– the passive fiber optic communication network of hybrid structure with time and wave multiplexing, providing data exchange channels between ACFOS and dispatch center, with possible use of wireless access networks;

– the artificial intelligence technology and processing of large amounts of data for operational decision-making to ensure the maximum level of environmental safety at various levels of the system.

Each of the above-mentioned tasks requires a scrupulous study and presentation of detailed results obtained at each stage of implementation, which is the subject of our further research. In this article, the authors did not go into detail about the measurements performed, but focused on the problem statements, excluding the last two. Expanded information will be the subject of future publications.

**Author Contributions:** Conceptualization, O.G.M. and A.Zh.S.; methodology, J.A.T.; software, B.I.V.; validation, T.A.A., S.M.R.H.H., A.A.K. and V.I.A.; formal analysis, O.G.M. and V.I.A.; investigation, A.A.K., K.A.L.; resources, J.A.T.; data curation, A.R.S.; writing—original draft preparation, O.G.M.; writing—review and editing, O.G.M.; visualization, A.Zh.S.; supervision, O.G.M.; project administration, O.G.M.; funding acquisition, J.A.T. All authors have read and agreed to the published version of the manuscript.

**Funding:** This work was financially supported by the Ministry of Science and Higher Education as part of the “Priority 2030” program.

**Conflicts of Interest:** The authors declare no conflict of interest.

## References

1. Jin, W.; Ho, H.L.; Cao, Y.C.; Ju, J.; Qi, L.F. Gas Detection with Micro- and Nano-Engineered Optical Fibers. *Optical Fiber Technology* **2013**, *19*, 741–759, doi:10.1016/j.yofte.2013.08.004.
2. Fei Ye; Li Qian; Bing Qi Multipoint Chemical Gas Sensing Using Frequency-Shifted Interferometry. *J. Lightwave Technol.* **2009**, *27*, 5356–5364, doi:10.1109/JLT.2009.2030776.
3. Gupta, N.; Sundaram, R. Fiber Optic Sensors for Monitoring Flow in Vacuum Enhanced Resin Infusion Technology (VERITy) Process. *Composites Part A: Applied Science and Manufacturing* **2009**, *40*, 1065–1070, doi:10.1016/j.compositesa.2009.04.022.
4. Suzumori, H.; Honma, S.; Morisawa, M.; Muto, S. Plastic Optical Fiber Sensor System for Detecting Multi-Point Gas Leakages.; Wang, A., Zhang, Y., Ishii, Y., Eds.; Beijing, China, November 29 2007; p. 682921.
5. Choi, J.C.; 이준규; Ho, K.S. A Multi-Channel Gas Sensor Using Fabry-Perot Interferometer-Based Infrared Spectrometer. *Journal of Sensor Science and Technology* **2012**, *21*, 402–407, doi:10.5369/JSST.2012.21.6.402.

6. Kou, J.-L.; Ding, M.; Feng, J.; Lu, Y.-Q.; Xu, F.; Brambilla, G. Microfiber-Based Bragg Gratings for Sensing Applications: A Review. *Sensors (Basel)* **2012**, *12*, 8861–8876, doi:10.3390/s120708861.
7. Sanoj Kumar Yadav; Nabamita Goswami; Ardhendu Saha Analysis of Multimode Interference Based More Sensitive Fiber Optic Methane Gas Sensor Using Bessel Beam with Wave Theory. In *Proceedings of the International Conference on Atomic, Molecular, Optical & Nano Physics with Applications*; Singh, V., Sharma, R., Mohan, M., Mehata, M.S., Razdan, A.K., Eds.; Springer Proceedings in Physics; Springer Singapore: Singapore, 2022; Vol. 271, pp. 633–638 ISBN 9789811676901.
8. Silva, S.; Frazão, O.; Viegas, J.; Ferreira, L.A.; Araújo, F.M.; Malcata, F.X.; Santos, J.L. Temperature and Strain-Independent Curvature Sensor Based on a Singlemode/Multimode Fiber Optic Structure. *Meas. Sci. Technol.* **2011**, *22*, 085201, doi:10.1088/0957-0233/22/8/085201.
9. Gong, Y.; Zhao, T.; Rao, Y.-J.; Wu, Y. All-Fiber Curvature Sensor Based on Multimode Interference. *IEEE Photon. Technol. Lett.* **2011**, *23*, 679–681, doi:10.1109/LPT.2011.2123086.
10. Wang, K.; Dong, X.; Kohler, M.H.; Kienle, P.; Bian, Q.; Jakobi, M.; Koch, A.W. Advances in Optical Fiber Sensors Based on Multimode Interference (MMI): A Review. *IEEE Sensors J.* **2021**, *21*, 132–142, doi:10.1109/JSEN.2020.3015086.
11. Wang, R.; Qiao, X. Gas Refractometer Based on Optical Fiber Extrinsic Fabry—Perot Interferometer With Open Cavity. *IEEE Photonics Technology Letters* **2015**, *27*, 245–248, doi:10.1109/LPT.2014.2365812.
12. Eom, J.; Park, C.-J.; Lee, B.H.; Lee, J.-H.; Kwon, I.-B.; Chung, E. Fiber Optic Fabry–Perot Pressure Sensor Based on Lensed Fiber and Polymeric Diaphragm. *Sensors and Actuators A: Physical* **2015**, *225*, 25–32, doi:10.1016/j.sna.2015.01.023.
13. Santos, J.S.; Raimundo, I.M.; Cordeiro, C.M.B.; Biazoli, C.R.; Gouveia, C.A.J.; Jorge, P.A.S. Characterisation of a Nafion Film by Optical Fibre Fabry–Perot Interferometry for Humidity Sensing. *Sensors and Actuators B: Chemical* **2014**, *196*, 99–105, doi:10.1016/j.snb.2014.01.101.
14. Zhao, Y.; Yuan, Y.; Gan, W.; Yang, M. Optical Fiber Fabry–Perot Humidity Sensor Based on Polyimide Membrane: Sensitivity and Adsorption Kinetics. *Sensors and Actuators A: Physical* **2018**, *281*, 48–54, doi:10.1016/j.sna.2018.08.044.
15. Huang, C.; Xie, W.; Yang, M.; Dai, J.; Zhang, B. Optical Fiber Fabry–Perot Humidity Sensor Based on Porous $Al_2O_3$ Film. *IEEE Photon. Technol. Lett.* **2015**, *27*, 2127–2130, doi:10.1109/LPT.2015.2454271.
16. Hoo, Y.L.; Jin, W.; Shi, C.; Ho, H.L.; Wang, D.N.; Ruan, S.C. Design and Modeling of a Photonic Crystal Fiber Gas Sensor. *Appl. Opt.* **2003**, *42*, 3509, doi:10.1364/AO.42.003509.
17. Arregui, F.J.; Claus, R.O.; Cooper, K.L.; Fernandez-Valdivielso, C.; Matias, I.R. Optical Fiber Gas Sensor Based on Self-Assembled Gratings. *J. Lightwave Technol.* **2001**, *19*, 1932–1937, doi:10.1109/50.971687.
18. Seitz, W.R.; Sepaniak, M.J. Chemical Sensors Based on Immobilized Indicators and Fiber Optics. *C R C Critical Reviews in Analytical Chemistry* **1988**, *19*, 135–173, doi:10.1080/10408348808542810.
19. Bremer, K.; Lewis, E.; Leen, G.; Moss, B.; Lochmann, S.; Mueller, I.A.R. Feedback Stabilized Interrogation Technique for EFPI/FBG Hybrid Fiber-Optic Pressure and Temperature Sensors. *IEEE Sensors Journal* **2012**, *12*, 133–138, doi:10.1109/JSEN.2011.2140104.
20. Ma, W.; Wang, R.; Rong, Q.; Shao, Z.; Zhang, W.; Guo, T.; Wang, J.; Qiao, X. CO2 Gas Sensing Using Optical Fiber Fabry–Perot Interferometer Based on Polyethyleneimine/Poly(Vinyl Alcohol) Coating. *IEEE Photonics J.* **2017**, *9*, 1–8, doi:10.1109/JPHOT.2017.2700053.
21. Tosi, D.; Poeggel, S.; Iordachita, I.; Schena, E. Fiber Optic Sensors for Biomedical Applications. In *Opto-Mechanical Fiber Optic Sensors*; Alemohammad, H., Ed.; Butterworth-Heinemann, 2018; pp. 301–333 ISBN 978-0-12-803131-5.
22. Morozov, O.G.; Sakhabutdinov, A.J. Addressed fiber bragg structures in quasi-distributed microwave-photonic sensor systems. *Comput. Opt.* **2019**, *43*, 535–543, doi:10.18287/2412-6179-2019-43-4-535-543.
23. Morozov, O.; Sakhabutdinov, A.; Anfinogentov, V.; Misbakhov, R.; Kuznetsov, A.; Agliullin, T. Multi-Addressed Fiber Bragg Structures for Microwave-Photonic Sensor Systems. *Sensors* **2020**, *20*, 2693, doi:10.3390/s20092693.

24. Agliullin, T.; Gubaidullin, R.; Sakhabutdinov, A.; Morozov, O.; Kuznetsov, A.; Ivanov, V. Addressed Fiber Bragg Structures in Load-Sensing Wheel Hub Bearings. *Sensors* **2020**, *20*, 6191, doi:10.3390/s20216191.
25. Agliullin, T.; Anfinogentov, V.; Misbahov, R.; Morozov, O.; Sakhabutdinov, A. Multicast Fiber Bragg Structures in Microwave Photonics Sensor Systems. *PTU* **2020**, *6*, 6–13, doi:10.31854/1813-324X-2020-6-1-6-13.
26. Ma, W.; Xing, J.; Wang, R.; Rong, Q.; Zhang, W.; Li, Y.; Zhang, J.; Qiao, X. Optical Fiber Fabry–Perot Interferometric $CO_2$ Gas Sensor Using Guanidine Derivative Polymer Functionalized Layer. *IEEE Sensors J.* **2018**, *18*, 1924–1929, doi:10.1109/JSEN.2018.2790973.
27. Martinez, A.; Dubov, M.; Khrushchev, I.; Bennion, I. Direct Writing of Fibre Bragg Gratings by Femtosecond Laser. *Electron. Lett.* **2004**, *40*, 1170, doi:10.1049/el:20046050.
28. Williams, R.J.; Krämer, R.G.; Nolte, S.; Withford, M.J. Femtosecond Direct-Writing of Low-Loss Fiber Bragg Gratings Using a Continuous Core-Scanning Technique. *Opt. Lett.* **2013**, *38*, 1918, doi:10.1364/OL.38.001918.
29. Ma, W.; Wang, R.; Rong, Q.; Shao, Z.; Zhang, W.; Guo, T.; Wang, J.; Qiao, X. $CO_2$ Gas Sensing Using Optical Fiber Fabry–Perot Interferometer Based on Polyethyleneimine/Poly(Vinyl Alcohol) Coating. *IEEE Photonics Journal* **2017**, *9*, 1–8, doi:10.1109/JPHOT.2017.2700053.
30. Peng, J.; Feng, W.; Yang, X.; Huang, G.; Liu, S. Dual Fabry–Pérot Interferometric Carbon Monoxide Sensor Based on the PANI/Co3O4 Sensitive Membrane-Coated Fibre Tip. *Zeitschrift für Naturforschung A* **2019**, *74*, 101–107, doi:10.1515/zna-2018-0453.
31. Kanawade, R.; Kumar, A.; Pawar, D.; Late, D.; Mondal, S.; Sinha, R.K. Fiber Optic Fabry–Perot Interferometer Sensor: An Efficient and Fast Approach for Ammonia Gas Sensing. *J. Opt. Soc. Am. B, JOSAB* **2019**, *36*, 684–689, doi:10.1364/JOSAB.36.000684.
32. Su, D.; Qiao, X.; Rong, Q.; Sun, H.; Zhang, J.; Bai, Z.; Du, Y.; Feng, D.; Wang, Y.; Hu, M.; et al. A Fiber Fabry–Perot Interferometer Based on a PVA Coating for Humidity Measurement. *Optics Communications* **2013**, *311*, 107–110, doi:10.1016/j.optcom.2013.08.016.
33. Xia, J.; Wang, F.; Luo, H.; Wang, Q.; Xiong, S. A Magnetic Field Sensor Based on a Magnetic Fluid-Filled FP-FBG Structure. *Sensors* **2016**, *16*, 620, doi:10.3390/s16050620.
34. Liang, H.; Jia, P.; Liu, J.; Fang, G.; Li, Z.; Hong, Y.; Liang, T.; Xiong, J. Diaphragm-Free Fiber-Optic Fabry-Perot Interferometric Gas Pressure Sensor for High Temperature Application. *Sensors* **2018**, *18*, 1011, doi:10.3390/s18041011.
35. Zhao, L.; Li, L. i. n.; Luo, A.; Xia, J.Z.; Qu, R.H.; Fang, Z. Bandwidth Controllable Transmission Filter Based on Moiré Fiber Bragg Grating. *Optik* **2002**, *113*, 464–468, doi:10.1078/S0030-4026(04)70192-8.
36. Sakhabutdinov, A.Z.; Anfinogentov, V.I.; Morozov, O.G.; Tunakova, Yu.A.; Danilaev, M.P.; Nureev, I.I.; Kuznetcov, A.A.; Lipatnikov, K.A.; Shagidullin, A.R.; Karimov, K.G.; et al. Digital twin of the Fabry-Perot sensor for greenhouse gas concentration monitoring. *Electronics, Photonics and Cyberphysical Systems* **2022**, *2*, 54–66.
37. Sakhabutdinov, A.J.; Morozov, O.G.; Ivanov, A.A.; Morozov, G.A.; Misbakhov, R.S.; Feofilaktov, S.V. Multiple Frequencies Analysis in Tasks of FBG Based Instantaneous Frequency Measurements. In Proceedings of the Proc SPIE Int Soc Opt Eng; Morozov O.G., Burdin V.A., Sultanov A.H., Andreev V.A., Bourdine A.V., Eds.; SPIE, 2018; Vol. 10774.
38. Tosi, D. Advanced Interrogation of Fiber-Optic Bragg Grating and Fabry-Perot Sensors with KLT Analysis. *Sensors* **2015**, *15*, 27470–27492, doi:10.3390/s151127470.
39. Tosi, D.; Perrone, G. Low-Cost, High Sensitivity, Signal Processing-Enhanced Fiber Bragg Grating Sensing System for Condition-Based Maintenance Application. *sens lett* **2011**, *9*, 1415–1422, doi:10.1166/sl.2011.1698.